

Integrated fracture characterization from seismic processing to reservoir modeling

Erika Angerer, Pierre Lanfranchi, CGG Technology London
Steve Rogers, Golder Associates UK

Abstract

Reliable sub-seismic scale fracture characterization requires a consistent workflow including wide-azimuth wide-offset data acquisition, azimuth-friendly and amplitude-preserved data pre-conditioning, robust attribute generation, and analysis of fracture-related azimuthal anisotropic effects. Using a Middle East dataset, we present an innovative workflow with the characteristic main features:

1. A recently developed geostatistical decomposition, allowing the separation of azimuthal seismic attributes into (1) a “geological” common part, (2) the azimuth-dependent information, and (3) random and organized noise.
2. An azimuth dependent 3D stratigraphic inversion, providing robust, layer-based elastic impedances.
3. An impedance (elliptical) curve-fitting procedure, extracting azimuthal anisotropy parameters.
4. A subsequent integration of inverted fracture parameters into a Discrete Fracture Network (DFN) model. The DFN approach allows the validation of the static model, through the simulated sampling of well fracture intersections. Furthermore, it provides an environment for simulating pressure transient responses and a route to upscaling grid cell permeabilities and reservoir modeling.

Introduction

Most methods for the characterization of azimuthal anisotropy are based on approximations of reflection coefficients (Rüger, 1998) and moveout velocities (Tsvankin, 1997) in fractured media. A similar azimuthal variation is derived for elastic impedances.

Coléou (2002) developed a geostatistical method aimed at decomposing 4D seismic data into (1) a geological “common part” and (2) the random and spatially organized noise such as acquisition footprints. Here, the technique is adapted to azimuth-limited seismic cubes to produce the noise-free anisotropic signal, which forms the input to the inversion of anisotropy parameters.

Conventionally, orientation and intensity seismic attributes are used qualitatively in reservoir characterization. Here, we propose to utilize these attributes directly in the generation of a reservoir fracture model. This is achieved with a Discrete Fracture Network (DFN) technology, an approach that explicitly represents key fracture elements within the rock mass (Dershowitz *et al* 1985). It is acknowledged that there may be other

routes by which seismic data may be taken to a reservoir model. However, using the DFN route, key aspects of fracture network geometry and connectivity are explicitly modeled and tested, providing a robust and demonstrable route from seismic attribute to a conditioned and geologically realistic fracture model.

Data pre-conditioning

We present a Middle East example from a high-fold OBC dataset that was acquired with crossline shooting to ensure a wide-azimuth, wide-offset distribution in the full-fold area. An “azimuth-friendly” processing sequence was applied, including dual sensor summation, deconvolution, high-resolution τ -p demultiple, high-order moveout correction and residual statics. A further important factor was the binning of the data into azimuth- and also angle-limited cubes. Macro-binning was required since the original bin size produces high S/N data only when all traces are stacked.

Geostatistical decomposition

The automatic factorial co-kriging technique developed by Coléou (2002) has been adapted for azimuthal anisotropy. In this case, azimuth-limited seismic cubes, or attributes derived from these (such as average amplitudes, NMO velocities, AVO attributes, elastic impedances, ...), form the multi-dimensional input.

From a set of orthogonal attributes, we can compute a “common part” which captures the invariant component (geology) of all these azimuthal attributes. By construction, this “common part” is noise free.

For each attribute A corresponding to azimuth ϕ with noise N it follows that:

$$A(\phi_1) + A(\phi_1 + 90^\circ) = 2A(45^\circ) + N_{A1}$$

$$A(\phi_2) + A(\phi_2 + 90^\circ) = 2A(45^\circ) + N_{A2}$$

The common part computed from these four azimuthal attributes provides the noise-free $A(45^\circ)$ (see Figure 1).

We then compute the following residuals:

$$R(\phi_1) = A(\phi_1) - A(45^\circ)$$

$$R(\phi_1 + 90^\circ) = A(\phi_1 + 90^\circ) - A(45^\circ)$$

Figure 1 shows that residual signals from orthogonal azimuths have the same magnitude (with opposite sign). The two calculated residuals contain the anisotropic component $An(\phi_1)$ as well as noise N_{ϕ_1} and N_{ϕ_1+90} , respectively:

$$R(\phi_1) = An(\phi_1) + N_{\phi_1}$$

$$R(\phi_1 + 90^\circ) = -An(\phi_1) + N_{\phi_1+90}$$

Computing again the common part of the residuals $R(\phi_1)$ and $R(\phi_1+90^\circ)$ gives the noise-free anisotropic component $An(\phi_1)$ of these two azimuths.

N_{ϕ_1} and N_{ϕ_1+90} contain the unpredictable parts varying between the different azimuths: spatially incoherent random noise as well as the acquisition footprint. Figure 2 illustrates the resulting components of this decomposition on one azimuthal attribute.

Stratigraphic Inversion of azimuth sectors

Once the data has been pre-processed in an “azimuth friendly” manner, we apply a layer-based inversion procedure to each azimuth sector. In order to ensure an overall consistency, the same initial model is used for all sectors. The 3D nature of the algorithm produces a set of impedances more robust and accurate than conventional AVO-based attributes. A note-worthy aspect of the layerbased approach, is its ability to automatically update the time thicknesses of the various azimuth sectors of the fractured layers during the inversion. An analysis of these variations gives estimates of travel time differences created by azimuthal anisotropy. Figure 3 shows the inverted impedances of one azimuth sector in the target area.

Anisotropy fitting of azimuthal attributes

The noise-free azimuth-dependent elastic impedances (compare to Figure 1) are now combined for the calculation of the orientation and magnitude of the azimuthal variation (Jenner, 2002). This is done by fitting an ellipse to the anisotropic response at each macro-bin, using a linear leastsquares algorithm. Error estimates can also be calculated. The results of this procedure are shown in Figure 4 and Figure 5 (map view). At its the well location, the inverted orientation lies within 5° of the dominant fracture orientation determined from FMI logs.

Data integration

The next step in the workflow is the integration of all available fracture information with the seismic attributes to build a Discrete Fracture Network (DFN) model. This information is gathered into a conceptual fracture model.

Conceptual model:

In using regional geological information (geomechanical model), outcrop studies, core samples, and well logs, the conceptual model identifies the dominant style of fracturing. The corresponding fracture pattern(s) (such as layer bound extensional joints, shear fractures,...) are used to constrain the DFN stochastic simulations.

Seismic attributes:

Seismic anisotropy attributes (intensity and orientation, shown on Figures 4 and 5), are used as a constraint to the stochastic simulation of fractures. Figure 6 shows a map view of one 3D realization. One of the key issues with

regards to seismically constrained fracture models, is the conversion of a single orientation vector into a geologically realistic fracture model. That is why during our stochastic simulation process, the conceptual model along with other information is used to constrain the orientation dispersion of the various realizations. This issue is critical as it controls the connectivity of the generated fracture network.

Validation:

Once a set of DFN models has been created, static validation is achieved in comparing actual and simulated fractures along the well path (Figure 7). The numerous realizations of the DFN process allow an assessment of the likely fracture connectivity and the size of connected fracture domains (Figure 7). These results can then be used for optimizing well placement in order to maximize the likely connection between the well and the fracture network.

Reservoir Simulation

Well testing represents the main method of sampling the fracture network away from the well. Wei *et al* (1998) have shown that the resultant pressure derivative curve from a pressure transient test characterizes the underlying fracture network. The DFN model is readily converted to a finite element flow grid, allowing the simulation of pressure transients (Figure 8). These simulations allow the determination of fracture transmissivities and the quantification of fracture pore volume. Also, they can be used to validate the conceptual fracture model by both static and dynamic means. Figure 9 shows that the DFN environment also provides a route to upscale the calibrated fracture model to cellular directional permeability values for direct inclusion in the reservoir simulation (Dershowitz *et al* 1998).

Conclusions

We present a workflow which enables us to extract robust attributes of azimuthal anisotropy from seismic data. These attributes are quantitatively integrated with available fracture information into a DFN model. DFN modeling includes the validation of the fracture conceptual model through well test simulation, as well as the derivation of cellular permeability and other engineering values for input to the reservoir simulator. This workflow provides a basis for planning field operations in fractured reservoirs in order to optimize production.

Acknowledgement

The authors would like to thank Didier Lecerf for his contributions to the geostatistical decomposition.

References

Coléou, T., 2002, Time-lapse filtering and improved repeatability with automatic factorial co-kriging (AFACK), 64th Mtg.: Eur. Assn. Geosci. Eng., Session: A018.

Dershowitz, W.S., B.M. Gordon, J.C. Kafritsas, and H.A. Herda, 1985. New Three-Dimensional Model for Flow in Fractured Rock. Proceedings, 17th International Congress of the International Association of Hydrogeologists, Tucson. Vol. 17, no. 1, p. 441-448.

Dershowitz, B., Lapointe, P., Eiben, T. & Wei, L. 1998. Integration of discrete fracture network methods with conventional simulator. SPE paper 49069.

Jenner, E., 2002, Azimuthal AVO: Methodology and data examples, TLE, Vol. 21, No. 8, 782-786.

Rüger, A., 1998, Variation of P-wave reflectivity with offset and azimuth in anisotropic media, Geophysics, Vol. 63, No. 3, 935-947.

Tsvankin, I., 1997, Reflection moveout and parameter estimation for horizontal transverse isotropy, Geophysics, 62, 614-629.

Wei, L., Hadwin, J., Chaput, E., Rawnsley, K. & Swaby, P. 1998. Discriminating fracture patterns in fractures reservoirs by pressure transient tests. SPE Paper 49233.

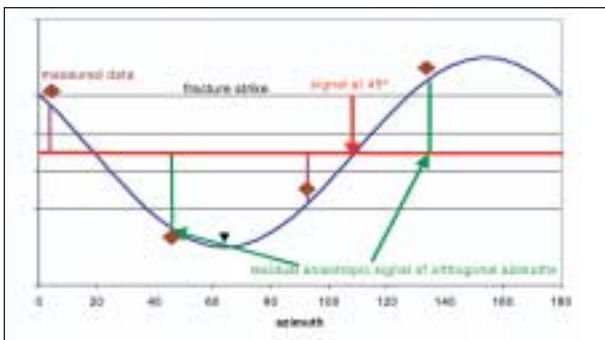


Figure 1: Azimuthal variation (blue) of anisotropic attributes; the red line indicates the 45° response; residuals of orthogonal attributes (green) contain the same anisotropic signal with opposite sign.

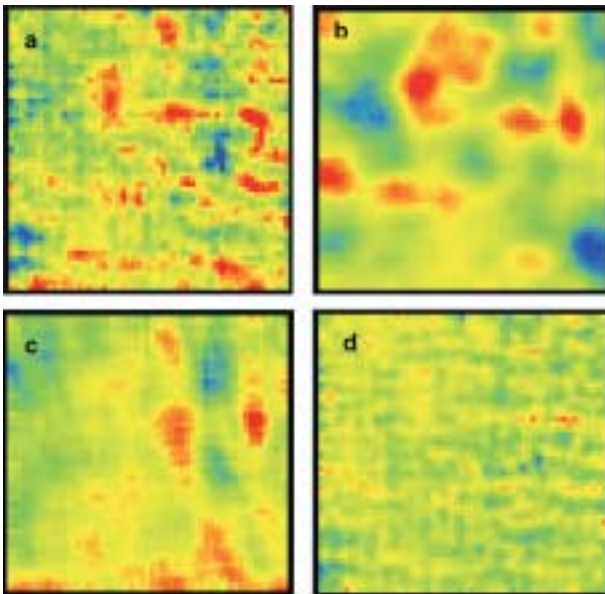


Figure 2: Map view of the geostatistical decomposition: an azimuthal attribute (a) is the sum of the common part (b), the anisotropic signal (c) and the noise (d).

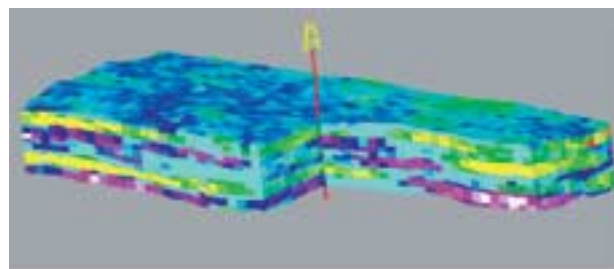


Figure 3: Layer-based stratigraphic inversion of one azimuth-sector.

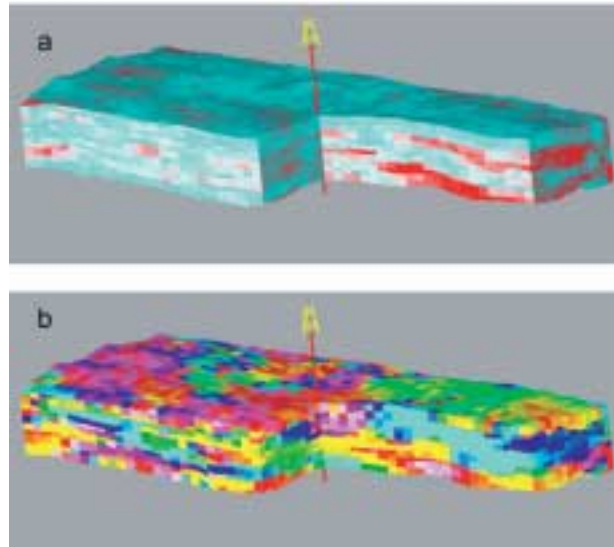


Figure 4: Layer-based anisotropic attributes, intensity (blue (low) – red (high)) (a) and orientation (b).

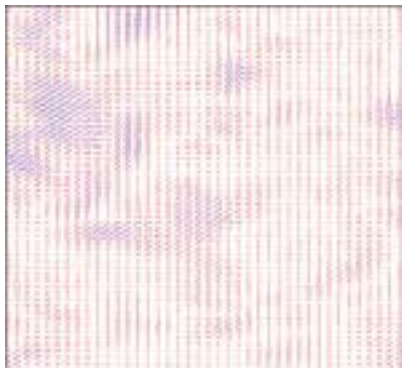


Figure 5: Layer-based anisotropy parameter map; the orientation of each line shows the main orientation and the length the relative intensity.

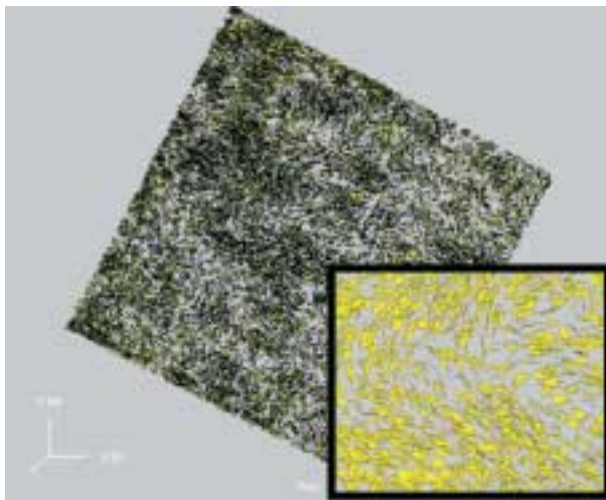


Figure 6: 25km² fracture model based on seismic attributes (Figure 5). Insert shows detailed variations in orientation and density.

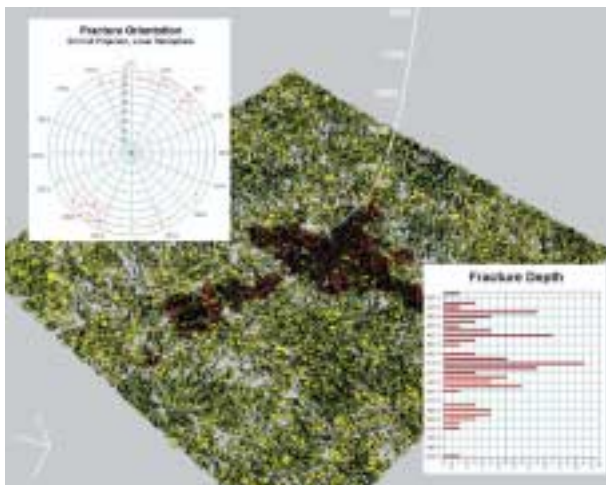


Figure 7: Sampling of the model allows simulated fracture intersections to be compared against actual well fracture information. The darker area represents those fractures connected indirectly to the well.

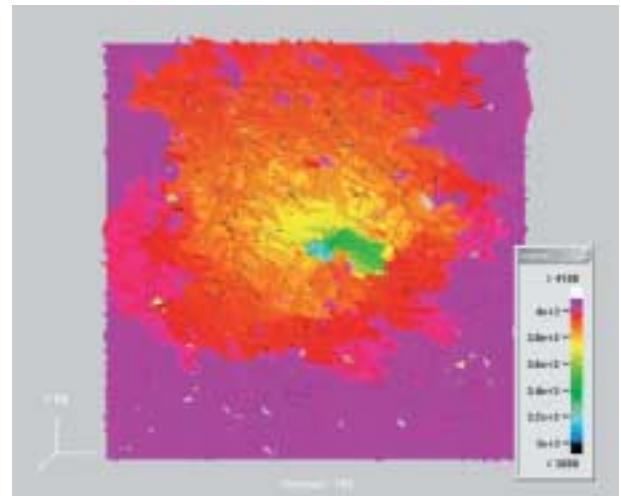


Figure 8: Conversion of the fracture model to a finite element flow grid allows the simulation of pressure transient tests through sections of the model. This model is 1km² and shows pressure diffusion after 100 hours.

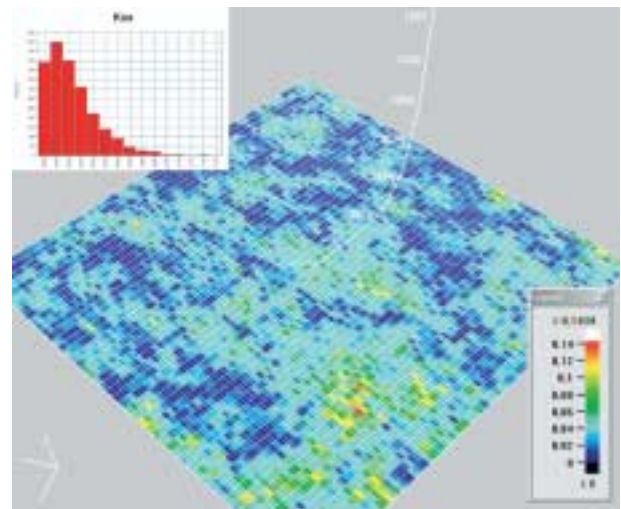


Figure 9: The DFN environment allows the ready calculation of grid scale permeability values.